JOURNAL OF INFORMATION SCIENCE AND ENGINEERING 35, 275-290 (2019)
DOI: 10.6688/JISE.201903_35(2).0002

Iris Recognition System Based on Fractal Dimensions Using Improved Box Counting

SAVIZ EBRAHIMI[1], MOHAMMAD BAGHER TAVAKOLI[1,+] AND FARBOD SETOUDEH[2]
[1]*Department of Electrical Engineering*
Islamic Azad University
Imam Khomeini Blvd, *Arak*, *38361-1-9131 Iran*
E-mail: {s-ebrahimi92; m-tavakoli[+]}@iau-arak.ac.ir
[2]*Department of Electrical Engineering*
Arak University of Technology
University Ave., *Arak*, *38131-4-1167 Iran*
E-mail: F.setoudeh@arakut.ac.ir

In this paper, a new approach based on an improved fractal dimensions (FDs) for an iris recognition system is proposed. Improved FDs, based on a differential box-counting (DBC) method were extracted from horizontal coefficients, vertical coefficients, and diagonal coefficients in different levels, by discrete wavelet transform. The CASIA iris images database was used to evaluate the algorithm; the simulation results are very promising.

Keywords: iris recognition, hough transform, fractal dimension, differential box-counting, Coif3 wavelets

1. INTRODUCTION

The French ophthalmologist Alphonse Bertillon appears to have been the first to propose the use of iris patterns as a basis for personal identification [1]. Biometrics is one of the most important and reliable methods of computer-aided personal identification, having a wide range of differing applications, such as national ID cards, visas and visa processing in government programs, and in the war against terrorism, as well as having personal applications in areas such as logical and physical access control. Among numerous biometrics approaches, iris recognition is known for its high reliability and accuracy, and so has emerged as being one of the important areas in the field.

Several iris recognition algorithms have previously been developed. Different approaches, such as integro-differential operator and two-dimensional Gabor Transform [2], the histogram-based model-fitting method and Laplacian Pyramid technique [3], zero crossings of wavelet transform [4], multi-channel Gabor filtering [5], circular symmetry filter [6], two-dimensional multi resolution wavelet transform [7], and two-dimensional Hilbert Transform [8] have been proposed. In the recent past, researchers have developed several mechanisms for matching the pattern that lies within the iris.

An iris recognition model based on sparse representation using compressive sensing and *k*-nearest sub space has been proposed in [9]. It combines the strength of three classifiers, *k*-nearest subspace, and sector based and cumulative sparse concentration index

Received September 26, 2017; revised July 2, 2018; accepted August 27, 2018.
Communicated by Wen-Liang Hwang.

and the weights of these classifiers are obtained by genetic algorithm. The method proposed in [10] is called RANSAC (Random Sample Consensus) that it fitting ellipse around non circular iris boundaries. Daugman's rubber sheet model is used for iris normalization and elliptic unwrapping, and correlation filter based matching for intra class and inter class distance evaluation. PSR (Peak Side Lobe Ratio) is the similarity measure used for matching templates.

A novel iris recognition method for iris dissimilarity computation applicable to mobile captured images is presented in [11]. It combines techniques from Computer Vision and Machine Learning. Several experiments using a combination of different image transformations and Machine Learning algorithms have been accomplished to select the best solution. The study in [12] presents a method that can be used for large database to reduce the matching time. This applied fractal dimension box counting method for classifying the iris images into four categories according to texture pattern. The method that is proposed in [13] is based on box-counting fractal dimension and low-high pass filters to extract iris features. The mention method can speed up a process by reducing a number of features. An iris recognition algorithm which adopts a bank of Gabor filters combined with the estimated fractal dimension is proposed in [14]. After the preprocessing procedure, the normalized effective iris region is decomposed according to different frequency regions by the multi-channel Gabor filters. The texture information of the filtered images is obtained via the differential box-counting method. In [15] the researchers present an iris recognition system based on the performance of Sparse Representation Coding followed by Spatial Pyramid Mapping technique for feature computation from iris pattern. To build the proposed system the existing Bio Hashing technique is modified using two different tokens: one is user specific and the other user independent. In [16], three discriminative feature selection strategies are described which are orientation probability distribution function (OPDF) based strategy to delete some redundant feature key points, magnitude probability distribution function (MPDF) based strategy to reduce dimensionality of feature element, and compounded strategy combined OPDF and MPDF to further select optimal sub feature and then a matching method based on weighted subregion matching fusion is used. The study in [17] presented a new feature and score fusion based iris recognition approach where voting method on Multiple Classifier Selection technique has been applied. Four Discrete Hidden Markov Model classifiers output, that is, left iris based unimodal system, right iris based unimodal system, left-right iris feature fusion based multimodal system, and left-right iris likelihood ratio score fusion based multimodal system, is combined using voting method to achieve the final recognition result. In [18], the researchers put forward a strategy to fuse different portions of iris based on machine learning method to evaluate local quality of iris. The normalized segmented iris is divided into multi-tracks and then each track is estimated individually to analyze the recognition accuracy rate then six local quality evaluation parameters are adopted to analyze texture information of each track. Particle swarm optimization is employed to get the weights of these evaluation parameters and corresponding weighted coefficients of different tracks and then all tracks' information is fused according to the weights of different tracks. An iris identification technique is presented in [19]. The iris is first segmented by using an edge detection algorithm. The segmented iris is transformed into a rectangular form. Described moments are extracted from the grayscale image which yields a feature vector containing scale, rotation, and translation invariant

moments. Images are clustered using the *k*-means algorithm and centroids for each cluster are computed at last Euclidean distance is used to matching. The concept of class-specific dictionaries is proposed for iris recognition in [20]. In mention research, the query image is represented as a linear combination of training images from each class. The well-conditioned inverse problem is solved using least squares regression and the decision is ruled in favor of the class with the most precise estimation. An enhanced modular approach is further proposed to counter noise due to imperfect segmentation of the iris region.

The hybrid approach of Fourier transforms and Bernstein polynomial for iris recognition has been proposed in [21]. Singular Value Decomposition (SVD) is used for iris image pre-processing. Circular Hough transform (CHT) and Canny edge detection (CED) are applied for iris image segmentation and Fourier transform and Bernstein polynomial have been applied to extract the iris features. At last Support Vector Machine (SVM) is used for image classification.

An iris recognition method as invention is presented in [22] which uses a matching pursuit algorithm to simplify the extraction and reconstruction of iris features and reduce the memory space required by each iris feature vector without the penalty of recognition accuracy. In mention method the Hough Transform is used to segment the region of an iris and then the iris region is normalized by Dougman rubber sheet model. In order to extract the essential iris features, a matching pursuit algorithm is used and then a set of feature vectors is obtained. The feature vector is expressed by a sequence of atoms, and each atom involves the information of base, amplitude and location. Thereby, only the most significant iris features are remained, and unimportant information is removed, and thus the required memory is reduced [22]. At last, to determine whether they match, the comparison between the feature vectors of two irises is performed [22].

Mandelbrot [23] was the first one who introduces fractals to estimate the roughness of a surface or texture. Fractal-based metrics capture texture properties, and a fractal dimension extracts roughness information from images, considering all available scales simultaneously. A fractal is an irregular geometric object with an infinite nesting of structure at all scales.

Single-scale features may not be sufficient to characterize the textures, so multiple-scale features are considered necessary for a more complete textural analysis [24]. Fractal Dimension (FD) is a useful feature for texture analysis, such as texture segmentation, shape classification, feature extraction, and graphic analysis, in numerous fields. The differential box-counting (DBC) method proposed by Sarkar and Chaudhuri is a generalization of the classical box-counting (BC) method to calculate the FD of gray-level images [25-32]. It has become a frequently used technique, due to its simplicity and automatic computability [33]. The human iris can be examined using fractal analysis because it has a rich self-similarity and random patterns. Extraction of unique features has a fundamental role in a recognition system so that accurate and strong information has a significant effect on the result of recognition. This paper presents a new method to extract the characteristics of the iris in order to be used in the iris recognition systems. This technique is based on FD approach that extracted biometric information contained in human iris patterns as unique features and followed by matching operations for recognition.

In this paper, a new method of iris recognition is presented, and an efficient BC-

based approach for the improvement of FD estimation accuracy in feature extraction of coif3 wavelet patterns atone, two, and three levels, is proposed. Wavelets are employed for the computation of single- and multiple-scale roughness features, due to their ability to extract information at different resolutions. In this model, the smallest number of boxes is used to cover the entire image surface at each selected scale, as required, thus obtaining a more accurate estimation in images that have sharp gray-level variations at the adjacent blocks, such as wavelet patterns of the iris template. In studies to date, the FDs that have been estimated by the DBC method may not be accurate and reliable (outside the range of between 2.0 and 3.0), so the proposed method may solve this problem and improve the iris verification algorithm. The FDS of sample images that have sharp gray-level variations were calculated to evaluate the improved DBC method, and the CASIA iris images database was used to evaluate the experimental results with regard to iris recognition performance.

2. FRACTAL DIMENSION ESTIMATION BASED ON DBC

2.1 The Original Box-Counting Method (DBC) and Similar Algorithms

The basic method used to estimate FD is based on the concept of self-similarity. The FD in Euclidean n-space is defined as

$$D = \frac{\log N_r}{\log 1/r}. \tag{1}$$

Where N_r is the least number of different copies of A in the scale r. The FD can only be calculated for deterministic fractals. With regard to an object with deterministic self-similarity, its FD is equal to its BC dimension. However, natural scenes and fractals are not classified in the ideal or deterministic fractals category [27]. The original method to estimate the fractal dimension based on BC is differential BC, which was introduced as follows [26]. Consider an image of size $M \times M$ as a three-dimensional, a surface with (x, y) that denotes pixel position on the image surface, and a third coordinate (z) that shows pixel gray-level. In the DBC method, the image surface is partitioned in non-overlapping blocks of size $s \times s$. The scale of each block is $r = s/M$, where $2 \le s \le M/2$ and s is an integer. N_r is the total number of boxes that cover the image in all scales and is calculated in the following manner.

Suppose a column of boxes of size $s \times s \times s'$ on each block, where s' is the height of each box and is defined as $G/s' = M/s$, where G is the total number of gray-levels. If the minimum and maximum gray-level in the (i, j)th block fall into the kth and lth boxes, respectively, the number of boxes covering this block will be calculated by Eq. (2).

$$n_r(i, j) = L - K + 1 \tag{2}$$

Where r denotes scale and N_r is counted by Eq. (3).

$$N_r = \sum n_r(i, j) \tag{3}$$

The FD can then be estimated from the least squares linear fit of $\log(N_r)$ versus $\log(1/r)$

[26]. Fig. 1 shows the determination of the number of boxes by the DBC method.

Jin *et al.* [34] proposed a relative DBC (RDBC) method, in which N_r is computed by Eq. (4).

$$N_r = \sum ceil[d_r(i,j)]/s' \tag{4}$$

Where $d_r(i, j)$ is defined as Eq. (5). In Eq. (5), $I_{\max}$ and $I_{\min}$ are the maximum and minimum values of intensity in the (i, j)th block, respectively; *ceil*[ ] denotes the ceiling function; and s' represents the height of each box. The fractal dimension can be estimated from the least squares linear fit of $\log(N_r)$ versus $\log(1/r)$.

$$d_r(i,j) = I_{\max} - I_{\min} \tag{5}$$

Chen *et al.* [35] described a shifting DBC (SDBC) algorithm, in which Eq. (6) is used to calculate n_r, and N_r is computed using Eq. (3).

$$n_r(i,j) = Ceil\left[\frac{I_{\max} - I_{\min} + 1}{s'}\right] \tag{6}$$

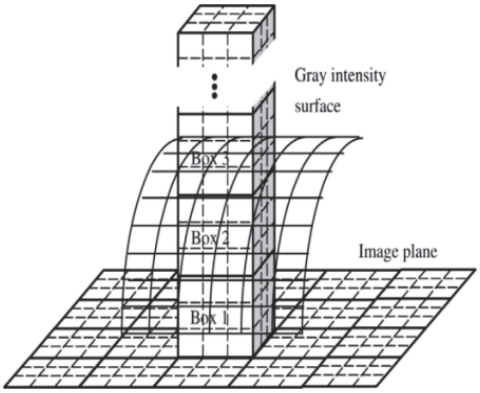

Fig. 1. Determination of the number of boxes using the differentiated box-counting method [29].

$I_{\max}$ and $I_{\min}$ refer to the maximum and minimum values of intensity in the (i, j)th block, respectively; *ceil*[] denotes the ceiling function; and s' is the height of each box. The fractal dimension can be estimated from the least squares linear fit of $\log(N_r)$ versus $\log(1/r)$.

Juan *et al.* [36] used the average gray level within the (i, j)th block to compute fractal dimensions. Here, $n_r(i, j)$ is defined by Eq. (7).

$$n_r(i,j) = \begin{cases} 1 + w \cdot (\bar{g} - g_{\min}) & (\bar{g} - g_{\min}) > (g_{\max} - \bar{g}) \\ 1 + w \cdot (g_{\max} - \bar{g}) & \text{else} \end{cases} \tag{7}$$

where w is the weight, presented in Eq. (8); N is the total number of pixels within a block; $N_{\min}$ is the number of pixels with a value falling between the minimum and mean values of the gray level; and $N_{\max}$ represents the number of pixels with a value that falls between the mean value and maximum values of the gray level. The total number of boxes cover-

ing an image plane is computed using Eq. (3), and the fractal dimension can be estimated from the least squares linear fit of $\log(N_r)$ versus $\log(1/r)$.

$$w = \begin{cases} N / N_{\min} & (\bar{g} - g_{\min}) > (g_{\max} - \bar{g}) \\ N / N_{\max} & \text{else} \end{cases} \tag{8}$$

2.2 The Improved Box-Counting Method (DBC*)

Use of the DBC method for images that have sharp gray-level variations at two adjacent blocks does not produce reliable results (outside the range between 2.0 and 3.0), so this problem is solved by shifting blocks in an image surface. In this method, the minimum number of boxes (n_r) in each block is calculated by Eq. (9).

$$n_r(i,j) = \begin{cases} Ceil(\frac{I_{\max} - I_{\min}}{h}) & I_{\min} \neq I_{\max} \\ 1 & I_{\min} = I_{\max} \end{cases} \tag{9}$$

Where $I_{\max}$ and $I_{\min}$ are the maximum and minimum gray-level of the image respectively. Ceil is ceiling function, which maps a real number to the smallest following integer and h is the height of each box.

In a similar manner to the DBC method, $M \times M$ is considered as the image size and $s \times s$ is the size of each block in an image surface, with h defined as

$$h = (G \times s)/M. \tag{10}$$

Where G is the total number of gray-scales and r is defined by Eq. (11) and presents the scale.

$$r = s/M \tag{11}$$

As mentioned previously, n_r is the number of the boxes that cover the block (i, j). After calculating n_r, the block in the image surface is shifted by Eq. (12), as presented in Fig. 2.

$$(i,j) \Rightarrow \begin{cases} (i+\alpha, j+\alpha) \text{ if } i = 0, j = 0 \\ (i-\alpha, j+\alpha) \text{ if } i = M, j < M \\ (i+\alpha, j-\alpha) \text{ if } i < M, j = M \\ (i-\alpha, j-\alpha) \text{ if } i = M, j = M \end{cases} \tag{12}$$

Where α is equal to 1. After shifting the blocks, the number of boxes in the shifted blocks is calculated again by Eq. (13), which is similar to Eq. (9), and n'_r indicates the number of boxes in each block after shifting.

$$n'_r(i,j) = \begin{cases} Ceil(\frac{I_{\max} - I_{\min}}{h}) & I_{\min} \neq I_{\max} \\ 1 & I_{\min} = I_{\max} \end{cases} \tag{13}$$

Eventually the final n_r, which is defined as n''_r, is computed by Eq. (14), and then N_r is calculated by Eq. (15). Finally, the FD can be estimated from the least squares linear fit of $\log(N_r)$ versus $\log(1/r)$.

$$n''_r = \min(n_r, n'_r) \tag{14}$$

$$N_r = \sum n''_r(i, j) \tag{15}$$

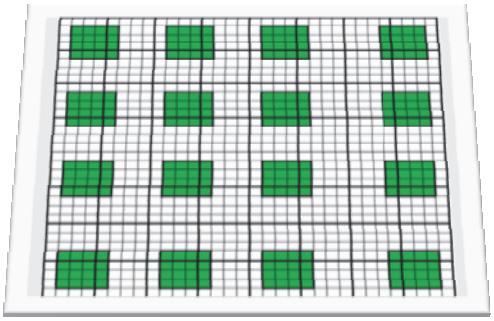

Fig. 2. Shifting the blocks in the image surface.

The FD of gray-level images is between 2.0 and 3.0; this range characterizes the degree of complexity. A greater FD indicates greater complexity or roughness. In order to prove this, the 2 and 3 bounds must be determined using the DBC method. The details are as follows. Consider an image of size 20×20 with one grayscale, so G in the DBC method is equal to 1 and $2 \le s \le M/2$, so $s = 2$, 4, 5, and 10. Then calculate n_r and N_r by Eqs. (5) and (6). Since $G = 1$, the number of the box in each block is 1, $n_r = 1$ for $r = 1/10$, 1/5, 1/4, and 1/2, and $N_r = 100$, 25, 16, and 4. Next, estimate the slope of $\log(N_r)$ versus $\log(1/r)$, which must be 2 in this case.

Now consider an image of size 20×20 with 256 gray-scale, so G in the DBC method is equal to 256 and $s = 2$, 4, 5, and 10. Then calculate n_r and N_r. Since $G = 256$, the number of boxes in each block is $n_r = 10$, 5, 4, and 2 for $r = 1/10$, 1/5, 1/4, and 1/2, and $N_r =$ 1000, 125, 64, and 8. Next, estimate the slope of $\log(N_r)$ versus $\log(1/r)$, which will be 3.

In fact, to determine this range, the complexity is specified as being the simplest when the image has only one gray-level and the most complex when there are 256 gray-levels in an image.

3. IRIS RECOGNITION BASED ON FRACTAL DIMENSION

A block diagram of the proposed iris recognition system is shown in Fig. 3. In this paper, the first stage of iris recognition is separating the exact iris region in a digital eye image based on Circular Hough transform [22]. The Circle Hough Transform (CHT) is a feature extraction approach to find circles in the desired image. The expected circles are produced by "voting" in the Hough parameter space and then save the local maxima in a so-called accumulator matrix. A circle is defined with three parameters: the center (a, b) and the radius R.

$$x = a + R\cos\theta \tag{16}$$

$$y = b + R\cos\theta \tag{17}$$

Following the change of θ from 0 to 360, a completed circle with radius R is created, thus the possible circles in the image are extracted by specifying three parameters of (x, y, R) [37]. The algorithm is described as follows:

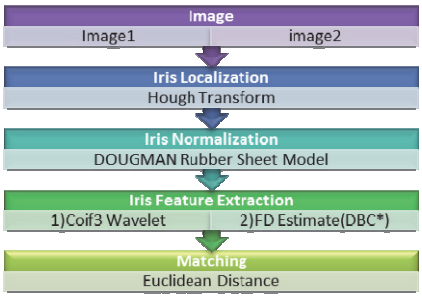

Fig. 3. Block diagram of the proposed iris recognition system.

1. Load an image
2. Detect edges and create a binary image
3. For every 'edge' pixel, create a circle in the a-b space
4. For every point on the circle in the a-b space, cast 'votes' in the accumulator cells
5. The cells with greater number of votes are the centers

To localize the iris ring, at first edge image is extracted by using canny edge detector. The iris region, shown in Fig. 4, can be approximated by two circles, one of them for the iris/sclera boundary and the other for iris/pupil boundary. The output of this stage in the iris recognition system has 6 parameters, including the radius and coordinates of the pupil center and the radius and coordinates of the iris center.

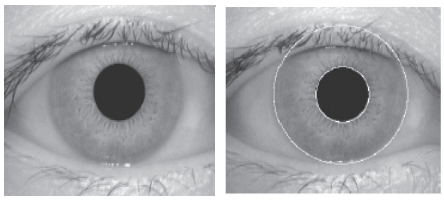

(a) (b)

Fig. 4. (a) An image of an iris; (b) The localized iris.

After the iris region was successfully extracted from an eye image, in next stage this region is changed into rectangle with fixed dimensions based on Dougman rubber sheet model [38]. This model is illustrated in Fig. 5, in this stage iris region transform from Cartesian coordinates into polar coordinates non-concentric normalized following as:

$$I(x(r, \theta), y(r, \theta)) \rightarrow I(r, \theta), \tag{18}$$

$$x(r, \theta) = (1 - r)x_p(\theta) + rx_l(\theta), \tag{19}$$

$$y(r, \theta) = (1 - r)y_p(\theta) + ry_l(\theta). \tag{20}$$

Where $I(x, y)$ is the iris region image, (x, y) are the original Cartesian coordinates, (r, θ) are the corresponding normalized polar coordinates. In iris image normalization, definition of the normalization parameters is effective on recognition accuracy.

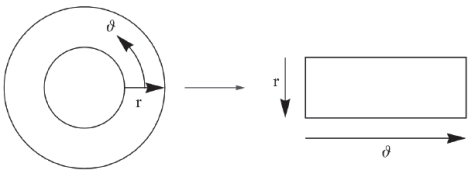

Fig. 5. The iris normalization process.

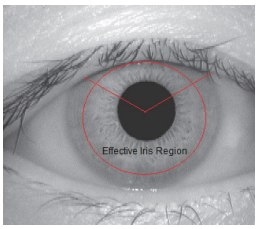

Fig. 6. The effective iris region.

Since the richest iris features are located in areas closer to the pupil, and according to various experiments, as shown in Fig. 6, two-thirds of the iris area near the pupil is considered, in this study; on the other hand, in order to removing the effect of the eyelashes and upper eyelid, the effective iris region is selected between $\frac{3\pi}{4}$ and $\frac{9\pi}{4}$ of segmented iris in other words, the features of this section are used in recognition. Eventually, the dimensions of the normalized iris pattern are 64×256.

After segmentation and normalization, the features of the normalized iris image are extracted. The final step of recognition algorithm is matching.

3.1 Proposed Iris Feature Extraction Method

Feature extraction plays a very *important role* in the recognition system. In this paper, a new method for iris feature extraction based on estimation of the FD of wavelet patterns, is described. After iris normalization, a *rectangular* block with a constant dimension (64×256) was generated. *This rectangular block* is called the iris template, and it was then enhanced using histogram equalization. Feature extraction from the enhanced iris template was considered by discrete wavelet transform. Coif3 was used as the mother wavelet at one, two and three levels. Using this method, the iris template was decomposed into horizontal coefficients, vertical coefficients, and diagonal coefficients. Fig. 7 shows the wavelet deconstruction at different levels. After feature extraction, the FDs were extracted from the horizontal coefficients, vertical coefficients, and diagonal coefficients at different levels.

The features *obtained from wavelet* coefficients had sharp gray-level variations, so the FD that was estimated using DBC did not appear be accurate and reliable. Therefore, improved DBC (DBC*) is applied in the proposed method, in order to solve this problem and improve identification accuracy. The improved DBC method calculates the smallest number of boxes to cover the entire image surface at each selected scale.

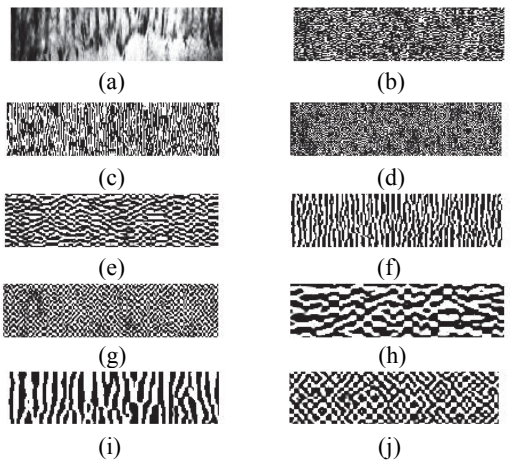

Fig. 7. Coif3 wavelet decomposition one, two, and three levels; (a) Iris template; (b), (c), (d) Horizontal, vertical, diagonal Coif3pattern in level 1; (e), (f), (g) Horizontal, vertical, diagonal Coif3 pattern in level 2; (h), (i), (j) Horizontal, vertical, diagonal Coif3 pattern in level 3.

The size of this feature is 64×256, and the pattern was divided into 16 regions in order to estimate the FD. Therefore, 32×32 image blocks were generated, as shown in Fig. 8. In order to calculate the FDs of these image blocks, the DBC* was used. This method was applied for all features *obtained from wavelet* coefficients. Putting together all fractal dimensions from the image blocks of all wavelet coefficients, the feature vector for an iris template image is obtained as Eq. (21) and 'T' is the transpose operator.

$$\textit{Iris Feature Vector} = [FD_{h11}, FD_{h12}, \ldots, FD_{h116}, \ldots, FD_{v21}, \ldots, FD_{d41}, \ldots, FD_{d416}]^T \quad (21)$$

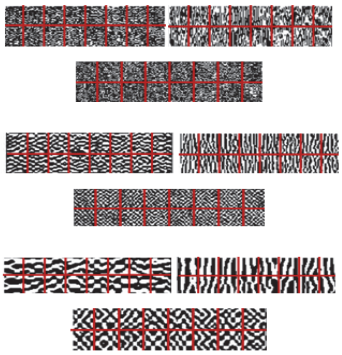

Fig. 8. Wavelet pattern images segmentation (32×32).

Finally, for matching in this method, Euclidean Distance was used. The Euclidean distance between points p and q is the length of the line segment connecting them. Therefore, two feature vectors obtained from two iris images were compared using Eq. (22) and p_i and q_i are corresponding elements belongs to two different feature vectors.

$$d(p,q) = \sqrt{\sum_{i=1}^{N} (p_i - q_i)^2} \tag{22}$$

4. EXPERIMENTAL RESULTS

4.1 Results of Image Fractal Analysis

In order to test the DBC* method, the images of Fig. 9 were considered. These types of images have sharp gray-level variations at adjacent blocks. E is the fit error that calculates the least squares linear fit of $\log(N_r)$ versus $\log(r)$. The lower fit error shows the better result. $y = c\,x + d$ is the fitted straight line and fit error (E) of (x, y) points is defined as Eq. (23) that y and x present $\log(N_r)$ and $\log(r)$ [26].

$$E = \frac{1}{n}\sqrt{\sum_{i=1}^{n} \frac{(dx_i + c - y_i)^2}{1+d^2}} \tag{23}$$

The FD and fit error results regarding the images shown in Fig. 9 were estimated by DBC, SDBC, RDBC, algorithm in [36] and DBC* methods, are shown in Table1 and Table 2 respectively . As illustrated in Fig. 10, some of the estimated fractal dimensions by the SDBC method and the presented method in [36] lie outside the range between 2.0 and 3.0, as shown in Section 2.2, the fractal dimension of a grayscale image is between 2.0 and 3.0, therefore this result is unreasonable, specifically. It clearly demonstrates that these methods cannot exactly estimate the FD of this kind of images which having gray-level variations at adjacent blocks, and so cannot estimate the roughness of them. The reason for this problem is that the boxes are under a specified box height and also are concentrated on specified place in intensity surface of image, so it caused some boxes will be over counted in box counting when the variations at adjacent two blocks. To resolve this, the boxes are shifted in DBC* method.

By considering Fig. 11, the fit error (E) for DBC and RDBC methods is more than DBC*, the fit error as a measurement parameter is very significant in order to evaluate the accuracy of the estimated fractal dimension, and the lower fit error shows the better result, in other words, the lower fit error determines higher accuracy. Because box counting methods are based on estimation and fitting methods, the lower fit error rate indicates the strength and desirability of the method in the correct counting of the boxes. According to the Fig. 10, the fit errors obtained from the DBC* method are lower than the other methods, because the number of boxes are counted accurately by this method for images with gray-level variation at adjacent blocks. Also by considering Fig. 10, the calculated fractal dimension by using DBC* method was more improved compared to DBC and RDBC methods.

Finally, it can be concluded that the DBC* method is more efficient than other DBC-based methods in estimating the fractal dimension of the images in Fig. 9. Therefore, it is more appropriate in iris recognition by the proposed method.

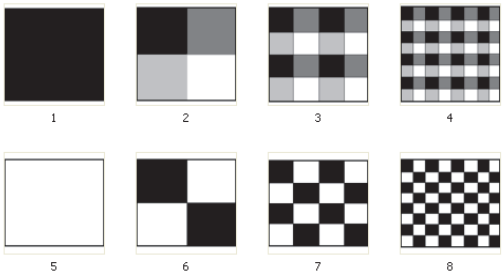

Fig. 9. Images with sharp gray-level variation.

Table 1. Results of fractal dimension estimation using different methods for images of Fig. 9.

Image	FD				
	DBC	RDBC	SDBC	[36]	DBC*
1	2	2	2	2	**2**
2	2.0075	2.0313	1.9784	1.8926	**2.0683**
3	2.1837	2.2235	2.1107	1.7346	**2.2838**
4	2.3207	2.3558	2.2164	1.7004	**2.4461**
5	2	2	2	2	**2**
6	2.0395	2.0659	1.9752	1.8577	**2.1119**
7	2.1636	2.1832	2.0541	1.7807	**2.2647**
8	2.3429	2.3776	2.2112	1.7457	**2.4599**

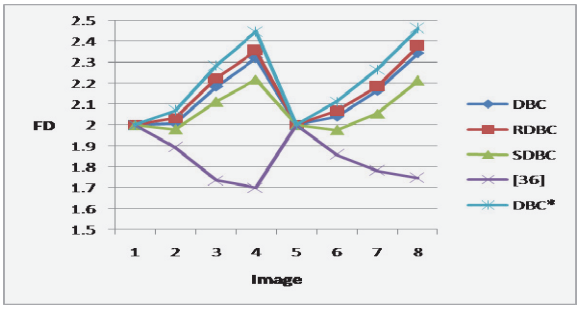

Fig. 10. The estimated fractal dimensions of the images in Fig. 9, using different methods.

Table 2. The computational fit errors (*E*) of FDs by using different methods for images of Fig. 9.

Image	E				
	DBC	RDBC	SDBC	[36]	DBC*
1	0	0	0	0	**0**
2	0.0084	0.0449	0.0116	0.0962	**0.0058**
3	0.0294	0.0359	0.0254	0.086	**0.0218**
4	0.0507	0.0459	0.0437	0.0775	**0.0332**
5	0	0	0	0	**0**
6	0.0174	0.0337	0.0214	0.0991	**0.0143**
7	0.0459	0.047	0.0377	0.0896	**0.0315**
8	0.0575	0.0536	0.0429	0.069	**0.0406**

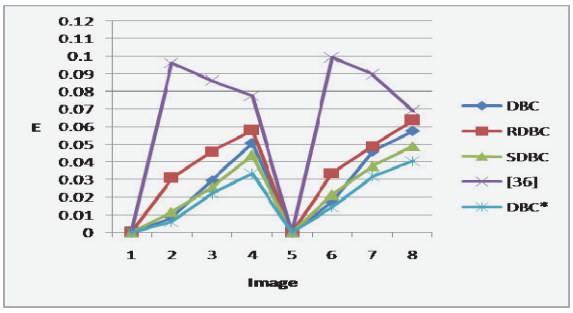

Fig. 11. The comparison of estimated FDs fit errors (*E*) by using different methods.

4.2 The Iris Recognition Results

In order to evaluate the performance of the proposed algorithm, the CASIA iris images database was used. This database has 756 iris images from 208 people. The simulation results are presented in Tables 3 and 4. Table 3 shows the results relating to when the original DBC and improved DBC* methods were used to extract the FD of the iris template before and after wavelet decomposition at levels one, two, and three. It is revealed that when *feature extraction* was used based on DBC* after wavelet decomposition, the *accuracy rate improved.*Table4 presents a comparison between different algorithms of iris identification based on fractal dimension and the proposed method. It is clear that the accuracy of the proposed method is promising.

Table 3. The results of the proposed algorithm, with and without Coif3 wavelet using the differential box-counting (DBC), RDBC and improved DBC (DBC*) methods.

Method	Accuracy Rate (%)
Using FD from iris template by DBC	92.5
Using FD from iris template by RDBC	89
Using FD from iris template by DBC*	96.5
Using FD from Coif3 patterns by DBC	90.5
Using FD from Coif3 patterns by RDBC	86.5
Using FD from Coif3 patterns by DBC*	98.5

Table 4. A comparison of different algorithms.

Method	Accuracy Rate (%)
FD[12]	92
FD(DBC)[13]	73.09
FD(DBC)+ High-Low Pass Filters[13]	91.22
Gabor filter+ FD[14]	96.6
Proposed Algorithm	98.5

5. CONCLUSIONS

An efficient algorithm for iris recognition based on the FDs of coif3 patterns, which reduces high computational complexities and improves the performance of traditional

recognition systems, has been developed. An improved differential box-counting method has been proposed, which shifts the block in the image surface, leading to more accurate estimations of FDs in wavelet patterns that have sharp gray-scaled variations at the adjacent blocks.

CASIA iris images database was used to evaluate the proposed algorithm, the experimental results show a high performance with regard to iris recognition applications.

REFERENCES

1. A. Bertillon, "la couleur de l'iris," *Revue Scientifique*, France, 1885.
2. J. G. Daugman, "High confidence visual recognition of persons by a test of statistical Independence," *IEEE Transactions on Pattern Analysis and Machine Intelligence*, Vol. 15, 1993, pp. 1148-1161.
3. P. J. Burt and E. H. Adelson, "The Laplacian pyramid as a compact image code," *IEEE Transactions on Communications*, Vol. 31, 1983, pp. 532-540.
4. W. W. Boles, "A security system based on human Iris identification using wavelet transform," in *Proceedings of the 1st IEEE International Conference on Knowledge-based Intelligent Electronic Systems*, 1997, pp. 532-540.
5. Y. Zhu, T. Tan, and Y. Wang, "Biometrics personal identification based on Iris patterns," in *Proceedings of the 15th IEEE International Conference on Pattern Recognition*, 2000, pp. 801-804.
6. L. Ma, Y. Wang, and T. Tan, "Iris recognition using circular symmetric filters," in *Proceedings of the 16th IEEE International Conference on Pattern Recognition*, 2002, pp. 414-417.
7. S. Lim, K. Lee, O. Byeon, and T. Kim, "Efficient Iris recognition through improvement of feature vector and classifier," *Electronics and Telecommunications Research Institute Journal*, Vol. 23, 2001, pp. 61-70.
8. C. L. Tisse, L. Martin, L. Torres, and M. Robert, "Person identification technique using human iris recognition," in *Proceedings of the 15th International Conference on Vision Interface*, 2002, pp. 294-299.
9. A. K. Bhateja, S. Sharma, S. Chaudhury, and N. Agrawal, "Iris recognition based on sparse representation and *k*-nearest subspace with genetic algorithm," *Pattern Recognition Letters*, Vol. 73, 2016, pp. 13-18.
10. T. Thomas, A. George, and K. P. I. Devi, "Effective Iris recognition system," *Procedia Technology*, Vol. 25, 2016, pp. 464-472.
11. N. Aginako, G. Echegaray, J. M. Martínez-Otzeta, I. Rodríguez, E. Lazkano, and B. Sierra, "Iris matching by means of machine learning paradigms: A new approach to dissimilarity computation," *Pattern Recognition Letters*, Vol. 91, 2017, pp. 60-64.
12. P. S. Patil, "Iris classification based on fractal dimension box counting method," *International Journal of Computer Applications*, Vol. 112, 2015, pp. 0975-8887.
13. A. Kraitong, S. Huvanandana, and S. Malisuwan, "A box-counting fractal dimension for feature extraction in Iris recognition," in *Proceedings of IEEE International Symposium on Intelligent Signal Processing and Communication Systems*, 2011, pp. 1-3.
14. C. C. Tsai, J. S. Taur, and C. W. Tao, "Iris recognition using Gabor filters and the fractal dimension," *Journal of Information Science and Engineering*, Vol. 25, 2009,

pp. 633-648.
15. S. Umer, B. C. Dhara, and B. Chanda, "A novel cancelable iris recognition system based on feature learning techniques," *Information Sciences*, Vol. 406-407, 2017, pp. 102-118.
16. Y. Chen, Y. Liu, X. Zhu, F. He, H. Wang, and N. Deng, "Efficient iris recognition based on optimal sub feature selection and weighted sub region fusion," *Scientific World Journal*, Vol. 2014, 2014, 19 pages.
17. M. R. Islam, "Feature and score fusion based multiple classifier selection for Iris recognition," *Computational Intelligence and Neuroscience*, Vol. 2014, 2014, 11 pages.
18. Y. Chen, Y. Liu, X. Zhu, H. Chen, F. He, and Y. Pang, "Novel approaches to improve iris recognition system performance based on local quality evaluation and feature fusion," *Hindawi Publishing Corporation the Scientific World Journal*, Vol. 2014, 21 pages.
19. Y. D. Khan, S. A. Khan, F. Ahmad, and S. Islam, "Iris recognition using image moments and *k*-means algorithm" *Hindawi Publishing Corporation the Scientific World Journal*, Vol. 2014, 2014, 9 pages.
20. I. Naseem, A. Aleem, R. Togneri, and M. Bennamoun, "Iris recognition using class-specific dictionaries," *Computers and Electrical Engineering*, 2016, pp. 1-16.
21. M. Ramya, V. Krishnaveni, and K. S. Sridharan, "Certain investigation on iris image recognition using hybrid approach of fourier transform and Bernstein polynomials," *Pattern Recognition Letters*, Vol. 94, 2017, pp. 1-9.
22. W.-G. Che, J.-L. Lin, W.-L. Hwang, and C.-L. Huang, "Iris recognition method utilizing matching pursuit algorithm," *National Chiao Tung University*, *U.S.A.*, 2011, US7, 920,724 B2.
23. B. B. Mandelbort and J. van Ness, "Fractional Brownian motions, fractional noises and applications," *SIAMR ev.*, Vol. 10, 1968, pp. 422-437.
24. D. Charlampidi and T. Kasparis, "Rotationally invariant texture segmentation using directional wavelet-based fractal dimensions," in *Proceedings of SPIE*, Vol. 4391, 2001, pp. 115-126.
25. N. Sarkar and B. B. Chaudhuri, "An efficient approach to estimate fractal dimension of textural images," *Pattern Recognition*, Vol. 25, 1992, pp. 1035-1041.
26. N. Sarkar and B. B. Chaudhuri, "An efficient differential box-counting approach to compute fractal dimension of image," *Transactions on Systems*, *Man and Cybernetics*, Vol. 24, 1994, pp. 115-120.
27. N. Sarkar and B. B. Chaudhuri, "Multi fractal and generalized dimensions of gray tone digital images," *Signal Processing*, Vol. 42, 1995, pp. 181-190.
28. S. Buczkowski, S. Kyriacos, F. Nekka, and L. Cartilier, "The modified box-counting method-analysis of some characteristic parameters," *Pattern Recognition*, Vol. 31, 1998, pp. 411-418.
29. J. Li, Q. Du, and C. Sun, "An improved box-counting method for image fractal dimension estimation," *Pattern Recognition*, Vol. 42, 2009, pp. 2460-2469.
30. A. K. Bisoi and J. Mishra, "On calculation of fractal dimension of images," *Pattern Recognition Letters*, Vol. 22, 2001, pp. 631-637.
31. M. K. Biswas, T. Ghose, S. Guha, and P. K. Biswas, "Fractal dimension estimation for texture images: a parallel approach," *Pattern Recognition Letters*, Vol. 19, 1998,

pp. 309-313.
32. X. C. Jin, S. H. Ong, and Jayasooriah, "A practical method for estimating fractal dimension," *Pattern Recognition Letters*, Vol. 16, 1995, pp. 457-464.
33. H. O. Peitgen, H. Jurgens, and D. Saupe, *Chaos and Fractals: New Frontiers of Science*, Springer, Berlin Heidelberg, 1992.
34. X. C. Jin, S. H. Ong, and Jayasooriah," A practical method for estimating fractal dimension," *Pattern Recognition Letter*, Vol. 16, 1995, pp. 457-464.
35. W. S. Chen, S. Y. Yuan, and C. M. Hsieh," Two algorithms to estimate fractal dimension of gray-level images," *Optical Engineering*, Vol. 42, 2003, pp. 2452-2464.
36. Y. Shi, S. Cheng, S. Quan, and T. Bai, "An anti-noise determination on fractal dimension for digital images," in *Proceedings of the 6th International Conference on Intelligent Systems and Knowledge Engineering*, Vol. 122, 2011, pp. 469-474.
37. R. C. Gonzalez and R. E. Woods, *Digital Image Processing*, Prentice Hall, NY, 2007.
38. J. G. Daugman, "How iris recognition works," *IEEE Transactions on Circuits and Systems for Video Technology*, Vol. 14, 2004, pp. 21-30.

Saviz Ebrahimi received her M.Sc. in Electrical Engineering from Azad University in 2009. She is currently a Ph.D. student of Electrical Department of Azad University. Her research interests include signal and image processing, biometrics, texture analysis, computer vision and pattern recognition.

Mohammad Bagher Tavakoli received his Ph.D. degree in Electrical Engineering from Science and Research branch of Azad University in 2012 and is currently an Assistant Professor at Electrical Engineering Department of Azad University. His research interests include linear integrated circuits.

Farbod Setoudeh received his Ph.D. degree in Electrical Engineering from Science and research branch of Azad University and is currently an Assistant Professor at Electrical Engineering Department of Arak University of Technology. His research interests include chaos, intelligent system, signal processing, and nonlinear system.